Electronic Supplementary Material (ESI) for New Journal of Chemistry.

Syntheses, structures, and magnetic properties of three new cyano-bridged heterobimetallic chains based on $[Fe(Tp^*)(CN)_3]^-$

Dapeng Dong,[a] Yanjuan Zhang, [b] Chengqi Jiao, [b] Liang Zhao, [b] Tao Liu*[b] Dedi Liu,[a] Zhenghua Li,[a] Jia Liu[a] and Dongping Liu*[a]

Supporting Information

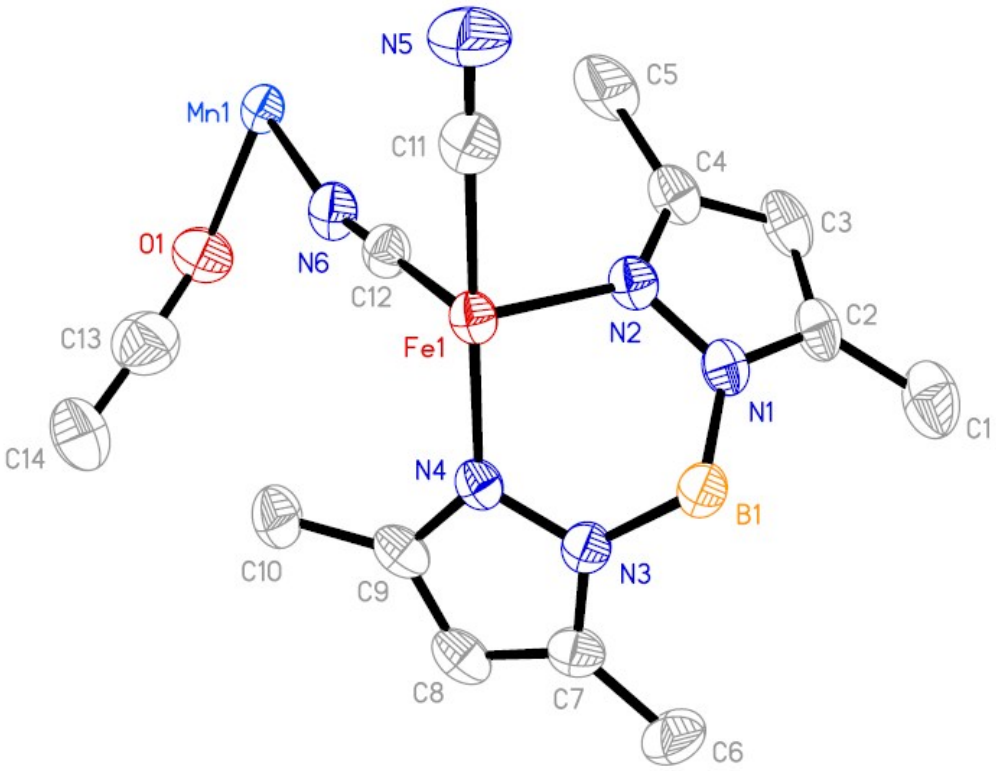

Fig S1. Asymmetric unit of compound **1** showing the atom labeling. Thermal ellipsoids are shown at the 30% probability level. All H atoms and water molecules are omitted for clarity.

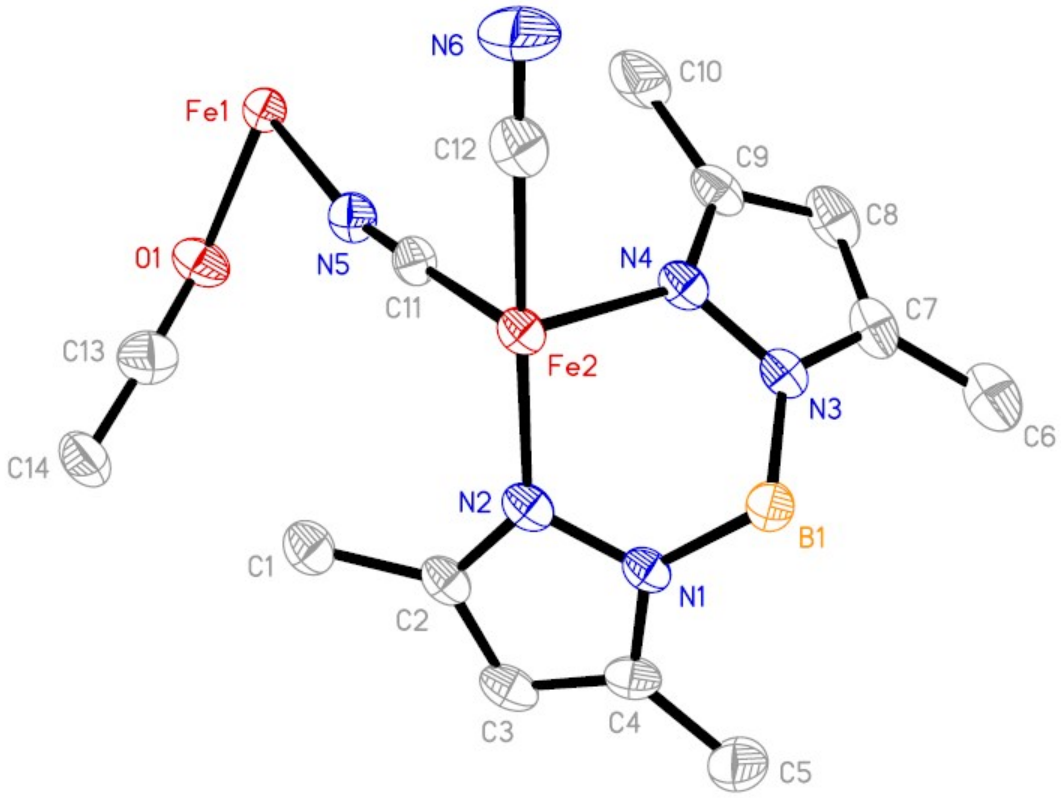

Fig S2. Asymmetric unit of compound **2** showing the atom labeling. Thermal ellipsoids are shown at the 30% probability level. All H atoms and water molecules are omitted for clarity.

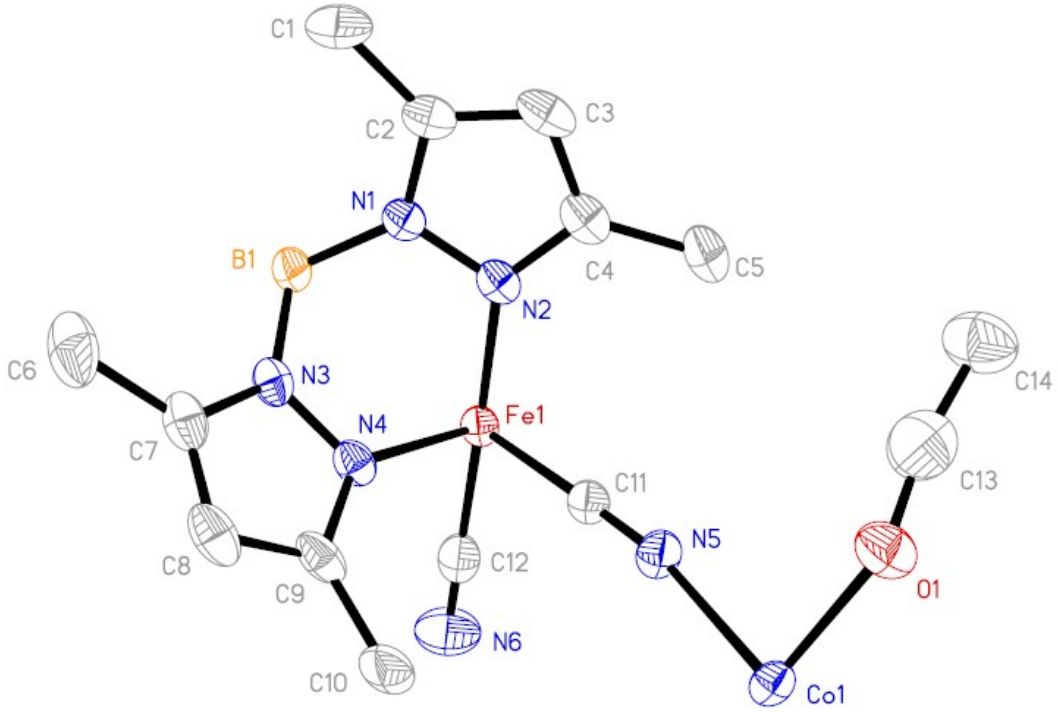

Fig S3. Asymmetric unit of compound **3** showing the atom labeling. Thermal ellipsoids are shown at the 30% probability level. All H atoms and water molecules are omitted for clarity.

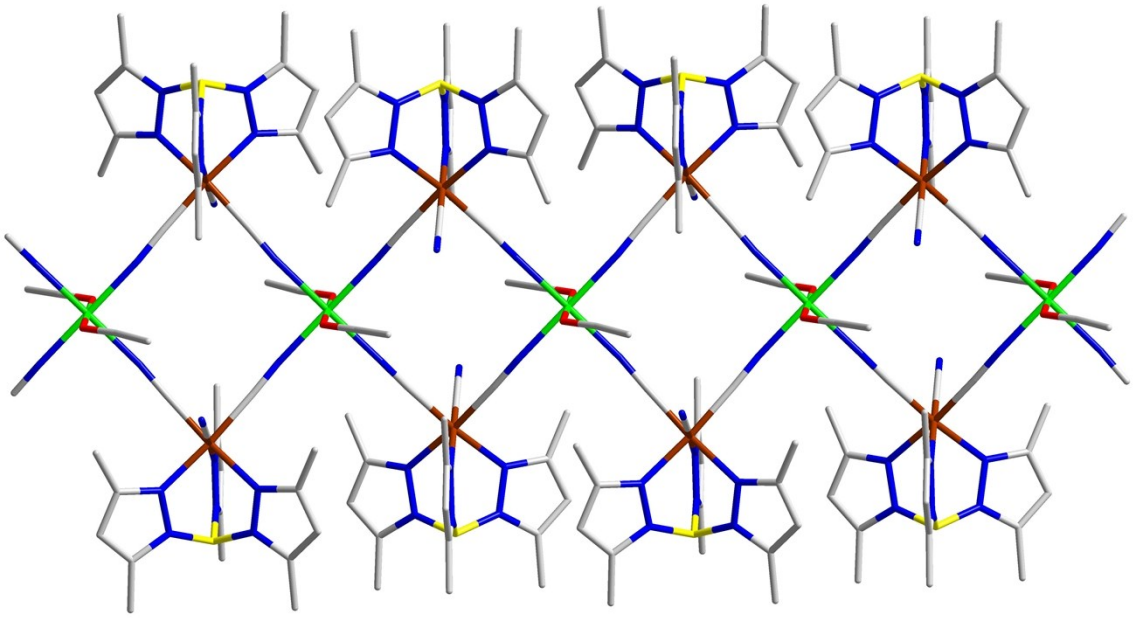

Fig. S4. Side view of a 1-D double-zigzag chain along the c-axis for compound **2**. H atoms and water molecules have been omitted for clarity. Atomic scheme: Fe(II), bright green; Fe(III), brown; C, gray; N, blue; B, yellow; O, red.

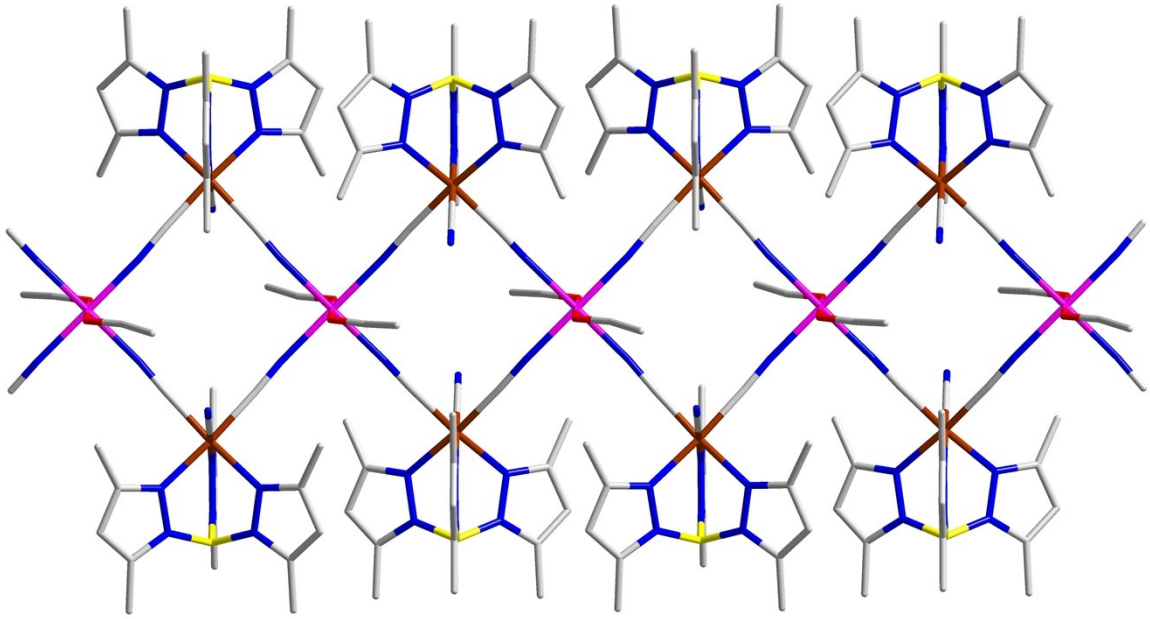

Fig. S5. Side view of a 1-D double-zigzag chain along the c-axis for compound **3.** H atoms and water molecules have been omitted for clarity. Atomic scheme: Co(II), pink; Fe(III), brown; C, gray; N, blue; B, yellow; O, red.

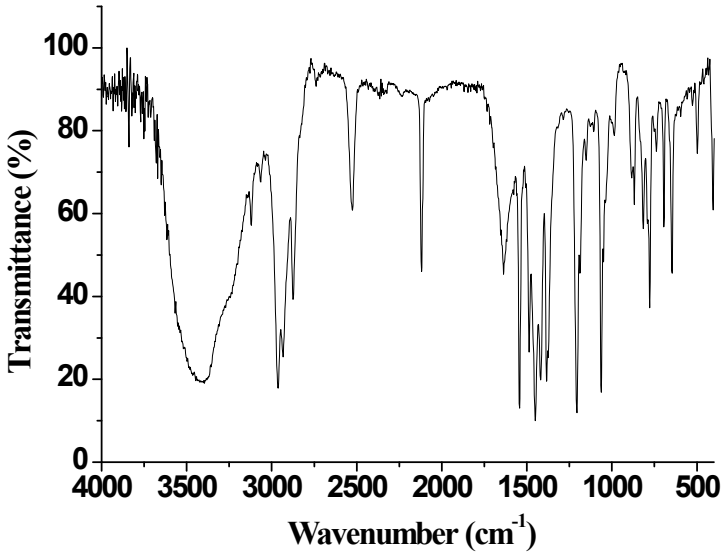

Fig S6. The IR spectrum of compound $[Bu_4N][Fe(Tp^*)(CN)_3]$.

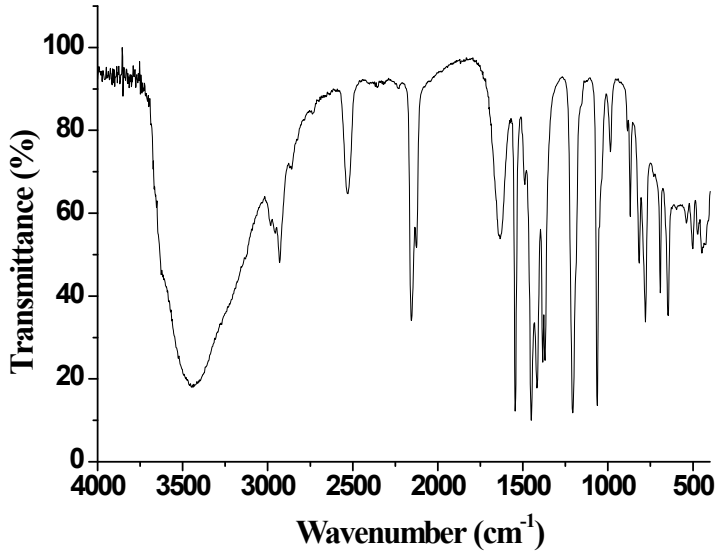

Fig S7. The IR spectra of compounds **1**.

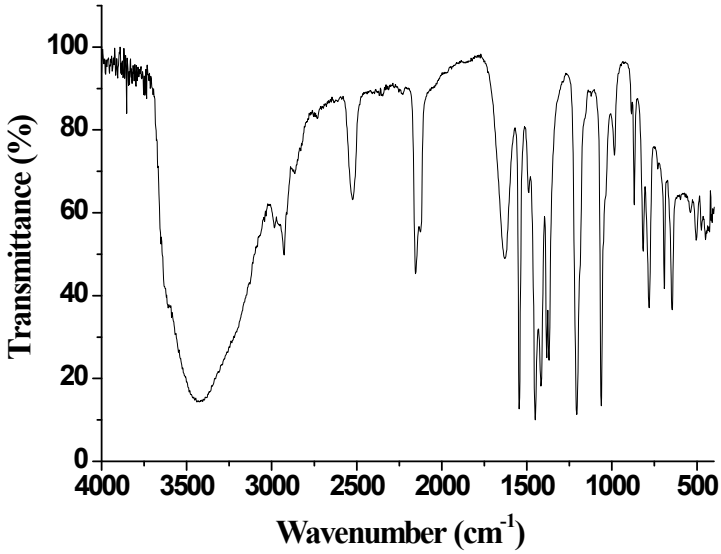

Fig S8. The IR spectra of compounds **2**.

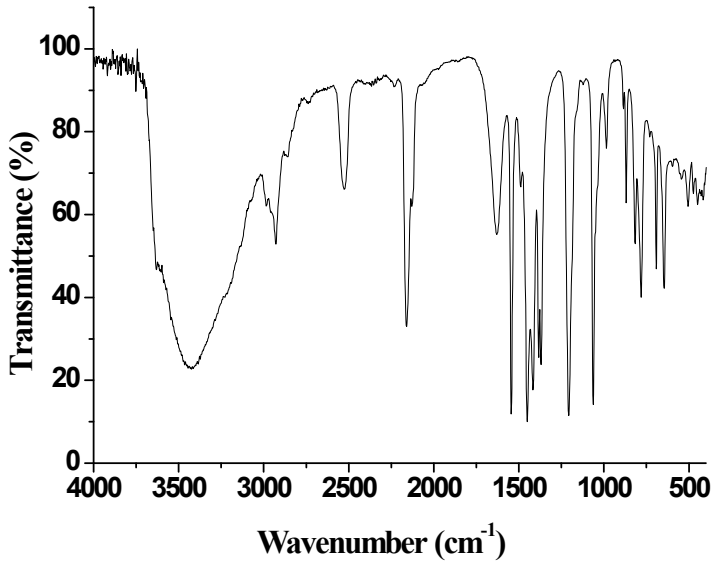

Fig S9. The IR spectra of compounds **3**.

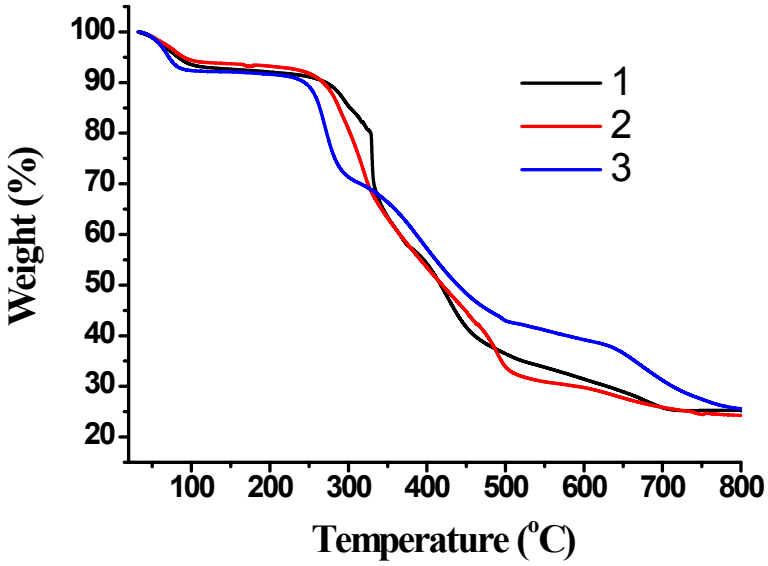

Fig S10. The TG curve of compound **1-3**.

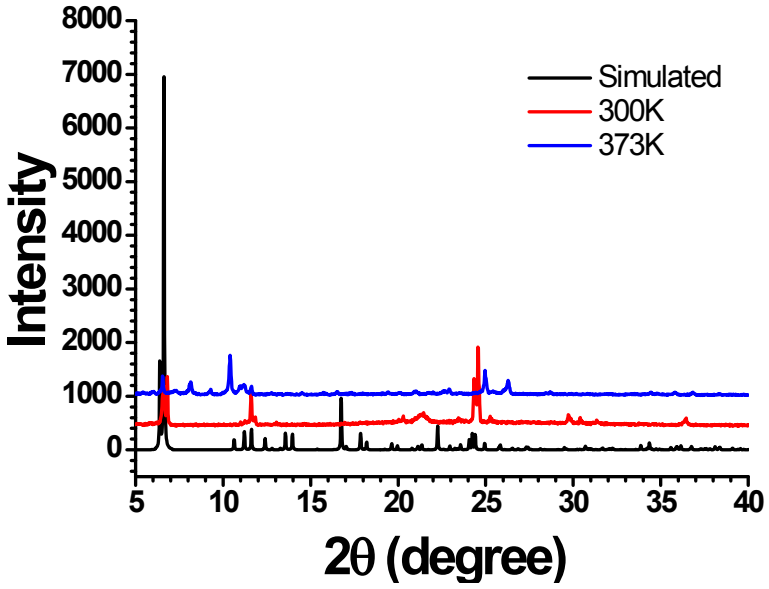

Fig S11. The simulated XRD pattern of compound **1** (up) and experimental powder XRD patterns at 300K (middle), 373K (down) of compounds **1**.

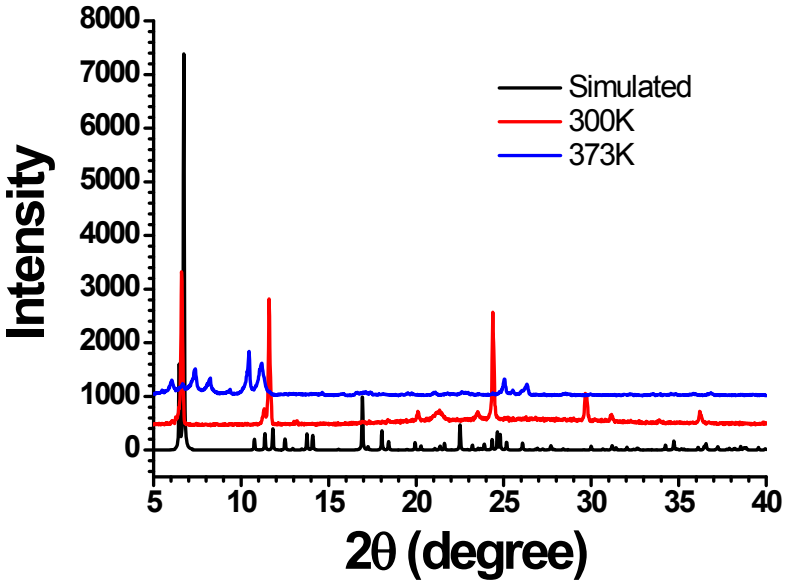

Fig S12. The simulated XRD pattern of compound **2** (up) and experimental powder XRD patterns at 300K (middle), 373K (down) of compounds **2**.

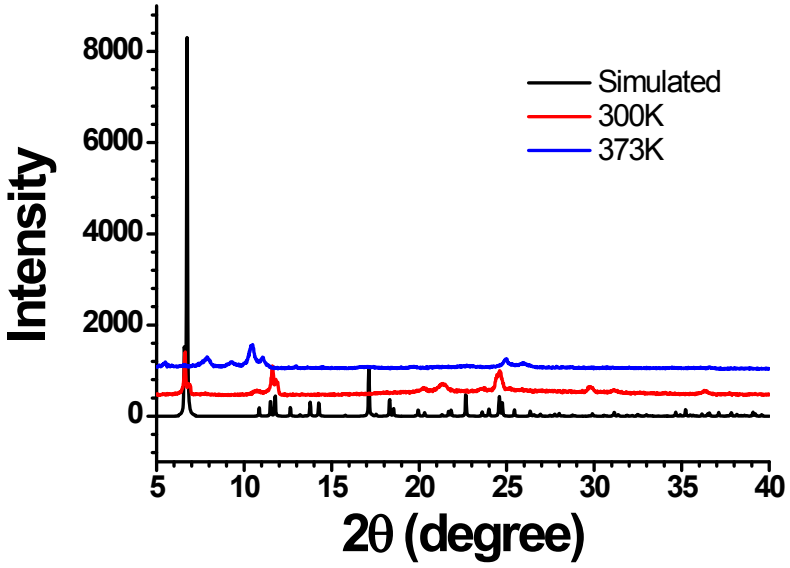

Fig S13. The simulated XRD pattern of compound **3** (up) and experimental powder XRD patterns at 300K (middle), 373K (down) of compounds **3**.

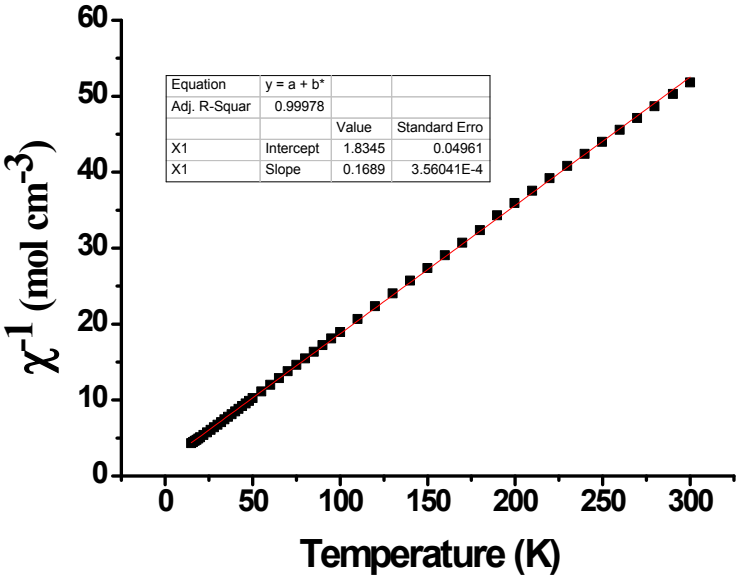

Fig. S14 Thermal variation of magnetic susceptibility, χ^{-1} vs T of compound **1** under an applied field of 1 kOe in the temperature range of 1.8–300 K.

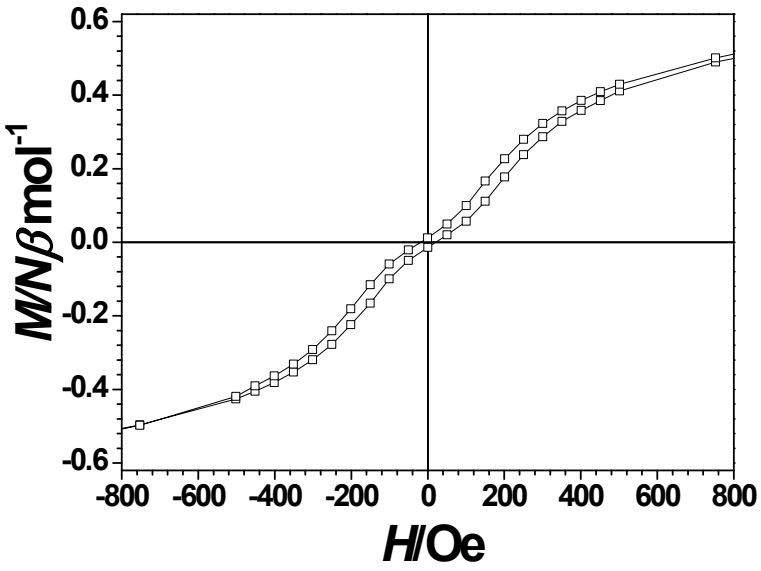

Fig S15. Field dependence of the magnetization showing the hysteresis loop for **1** at 1.8 K.

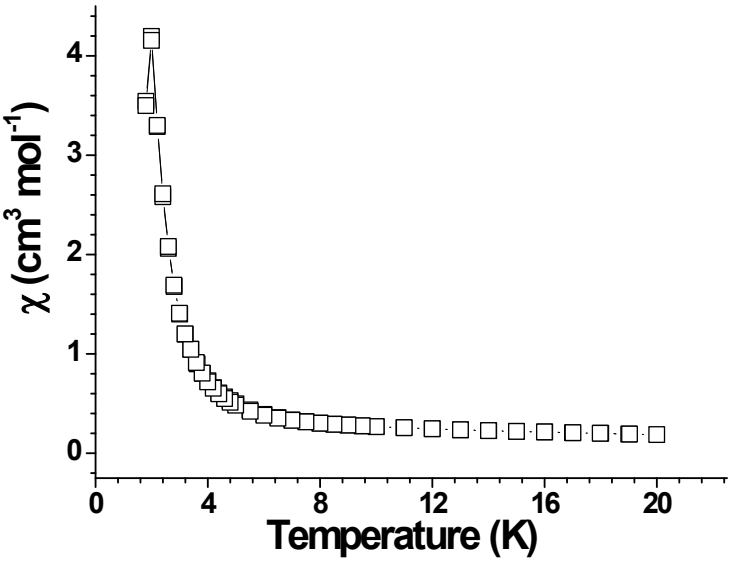

Fig. S16 The coincident ZFC and FC magnetization curves of **1** at 100 Oe.

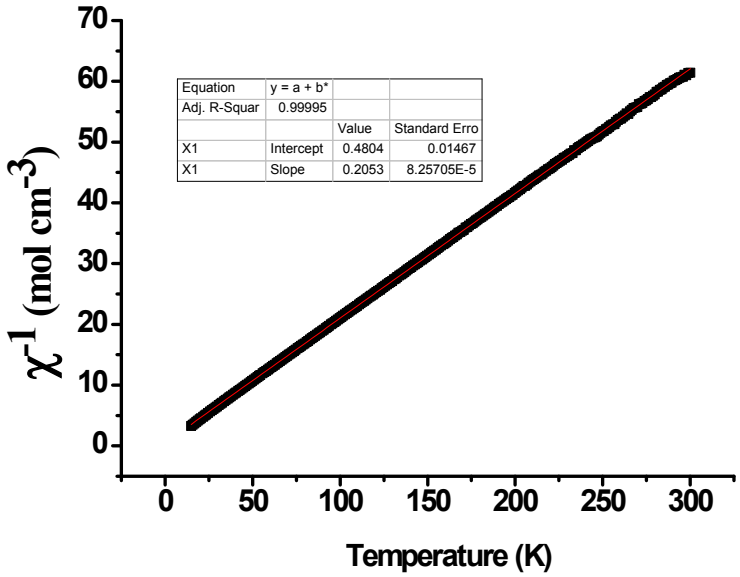

Fig. S17 Thermal variation of magnetic susceptibility, χ^{-1} vs T of compound **2** under an applied field of 1 kOe in the temperature range of 1.8–300 K.

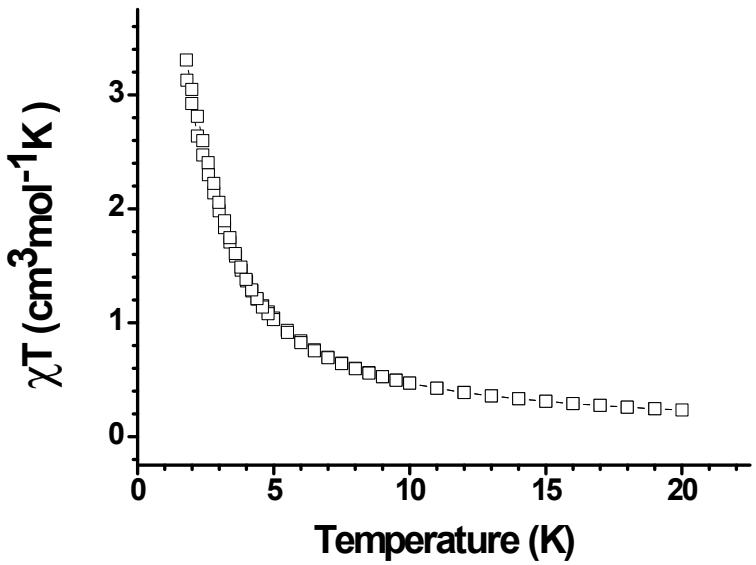

Fig. S18 The coincident ZFC and FC magnetization curves of **2** at 100 Oe.

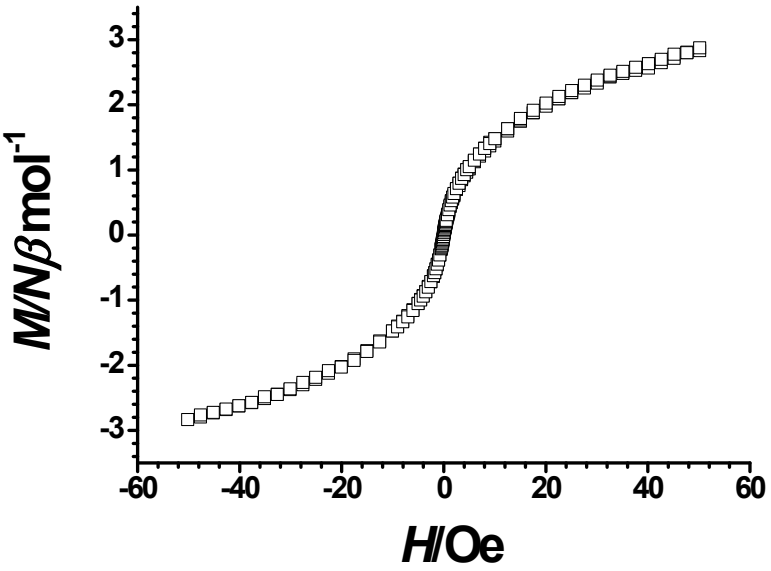

Fig S19. Field dependence of the magnetization showing the hysteresis loop for **2** at 1.8 K.

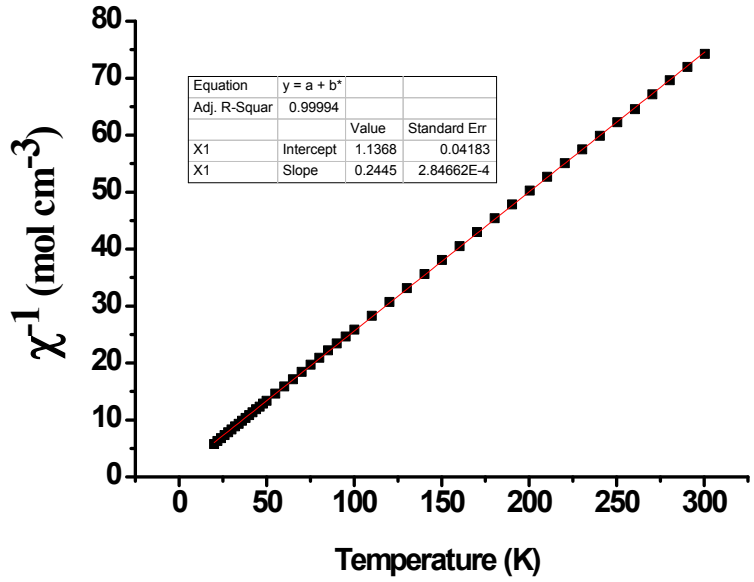

Fig. S20 Thermal variation of magnetic susceptibility, χ^{-1} vs T of compound **3** under an applied field of 1 kOe in the temperature range of 1.8–300 K.

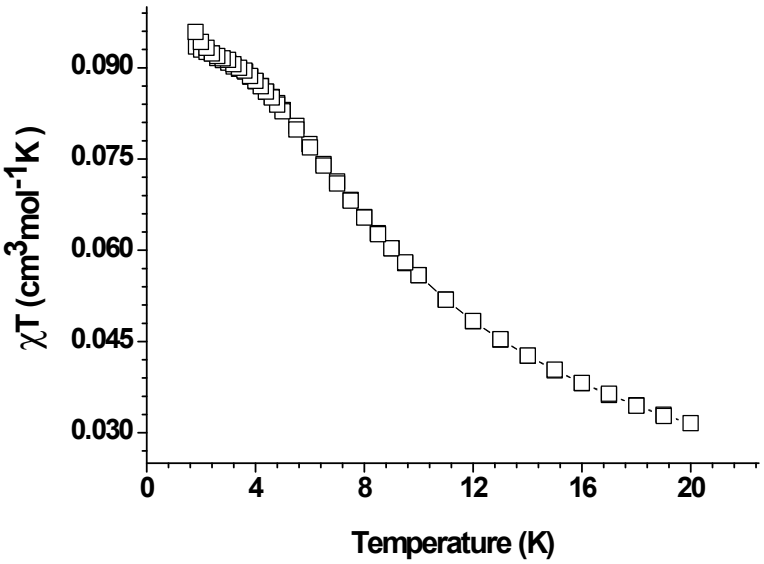

Fig. S21 The coincident ZFC and FC magnetization curves of **3** at 100 Oe.